2*p* x-ray absorption of free transition-metal cations across the 3*d* transition elements: Calcium through copper

K. Hirsch,[1,2] V. Zamudio-Bayer,[1,2] F. Ameseder,[1,2] A. Langenberg,[1,2] J. Rittmann,[1,2] M. Vogel,[1] T. Möller,[2] B.v. Issendorff,[3] and J. T. Lau[1,*]

[1]*Institut für Methoden und Instrumentierung der Forschung mit Synchrotronstrahlung, Helmholtz-Zentrum Berlin für Materialien und Energie GmbH, Albert-Einstein-Straße 15, 12489 Berlin, Germany*

[2]*Institut für Optik und Atomare Physik, Technische Universität Berlin, Hardenbergstraße 36, 10623 Berlin, Germany*

[3]*Fakultät für Physik, Universität Freiburg, Stefan-Meier-Straße 21, 79104 Freiburg, Germany*

(Received 21 March 2012; published 1 June 2012)

Experimental 2*p* x-ray-absorption spectra of 3*d* transition-metal cations in their electronic ground states were obtained in photoion-yield detection. Individual transitions are assigned within the $Z+1$ approximation and Hartree-Fock calculations, which reproduce the experimental spectra with good agreement. For 3*d* transition metals, 2*p* x-ray-absorption spectra are nearly identical for atoms and cations with equal 3*d* electron configurations. The oscillator strengths of $2p \rightarrow 3d$ transitions in 3*d* transition-metal cations are proportional to the number of unoccupied 3*d* states in accordance with bulk data. The "continuum step" does not coincide with the direct 2*p* photoionization threshold but is related to resonant transitions into Rydberg states. For nickel cations, a 2*p* core-hole lifetime of 1.6 ± 0.1 fs is derived from the natural linewidth, which is 0.1–0.2 eV smaller than for nickel adatoms and bulk because of the absence of inhomogeneous broadening.

DOI: 10.1103/PhysRevA.85.062501 PACS number(s): 32.30.Rj, 32.80.Aa, 32.80.Fb, 37.10.Ty

I. INTRODUCTION

X-ray-absorption spectroscopy is widely used as a probe of the unoccupied valence-electron density of states in the investigation of physical and chemical properties of elements and compounds [1–3]. For 3*d* transition metals in particular, the analysis of $2p \rightarrow 3d$ x-ray absorption [4] often serves to identify the local atomic character of electronic states in dilute impurity atoms, adatoms on thin films and surfaces [5,6], or transition-metal ions in compounds [7,8] which show sufficiently strong multiplet splitting to render fingerprint analysis successful. To this end, atomic Hartree-Fock calculations [3,9–12] are widely used to analyze 2*p* excitations of 3*d* transition metals, but no experimental 2*p* reference spectra of isolated 3*d* transition-metal ions were available so far.

Up to date, most inner-shell photoionization studies on free metal atoms or ions were performed with merged-beam [13–19] or crossed-beam [20–29] techniques. While merged-beam studies extensively cover 3*p* photoionization of 3*d* transition metals [15] and even allow for the determination of absolute x-ray-absorption cross sections, they have not yet been applied to 2*p* photoionization of 3*d* transition-metal ions. In crossed-beam experiments, 2*p* x-ray absorption has been studied in free atoms across the first-row transition metals [20–29]. These experiments are challenging even at third-generation synchrotron radiation facilities, mainly because of low target density. This lack of target density can, however, be overcome by using ion traps, which have been introduced recently to core-level photoexcitation studies of atomic and molecular ions [30–34]. For state-specific x-ray-absorption studies, these ion traps can even be exploited to prepare ions in their electronic ground states by relaxing long-lived metastable states [31]. Here we make use of a linear ion trap to obtain experimental 2*p* photoionization spectra of 3*d* transition-metal cations in their ground states and in the absence of any crystal field.

II. EXPERIMENTAL SETUP

Photoionization at the 2*p* edges of 3*d* transition-metal cations was recorded in a linear ion trap setup, which has already been described in the investigation of size-selected transition-metal cluster cations [33–38]. This setup combines an intense metal ion source with high-transmission ion guides and a linear radio-frequency quadrupole ion trap for core-level photoionization, detected via ion-yield spectroscopy.

In brief, 3*d* transition-metal cations were generated in a liquid-nitrogen-cooled magnetron ion source by argon sputtering of high-purity transition-metal targets in a mixed helium and argon atmosphere at 0.1–1 mbar. At the exit aperture of the ion source, transition-metal cations are guided by a radio-frequency hexapole ion guide through a differential pumping stage into a radio-frequency quadrupole mass filter which selects the ions of interest. The mass-selected ion beam is then deflected by a static electric quadrupole field and focused by an electrostatic ion lens onto the entrance aperture of a cryogenic linear radio-frequency quadrupole ion trap, filled with liquid-nitrogen-cooled helium buffer gas for enhanced trapping efficiency and thermalization. The ion trap is loaded continuously with transition-metal ions to the space-charge limit, generating a constant target density of $\approx 5 \times 10^7$ ions cm^{-3}. The incident soft-x-ray radiation beam is aligned coaxially with the ion trap to ensure maximum overlap of the photon beam and 1×1 mm^2 ion column over a path length of 20 cm, defined by the ion trap dimensions. During data acquisition, the incoming photon flux is recorded with a GaAsP photodiode mounted behind the ion trap, and all x-ray-absorption spectra shown here are normalized to

*tobias.lau@helmholtz-berlin.de

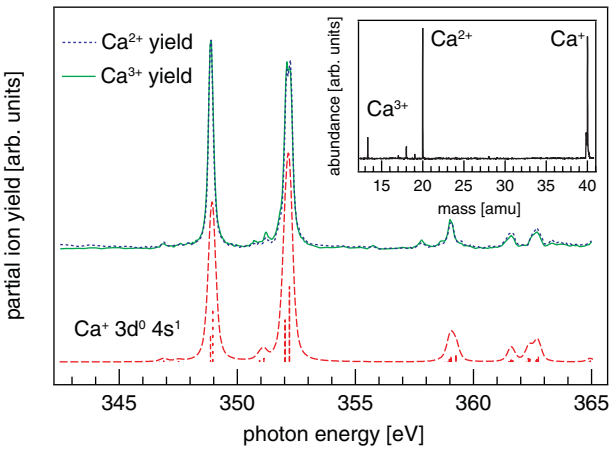

FIG. 1. (Color online) Experimental partial ion-yield signals of Ca^{2+} (dotted line) and Ca^{3+} (solid line) product ions generated in photoionization of Ca^{+} parent ions at the calcium $L_{2,3}$ edges, scaled to the same intensity and compared to the theoretical (dashed line) Ca^{+} $2p$ x-ray-absorption spectrum for the $[Ar]3d^{0}4s^{1}$ initial state configuration. Inset: $2p$ photoionization mass spectrum averaged over all photon energies. Photoionized water molecules from residual gas are also present in the mass spectrum.

the photon flux after correction for the GaAsP photodiode quantum efficiency.

III. 2*p* X-RAY ABSORPTION OF FIRST-ROW TRANSITION METAL IONS

A. Ion-yield spectroscopy

All $2p$ photoionization spectra shown here were recorded in photoion-yield detection mode by monitoring the product-ion intensity. Following $2p$ x-ray absorption, the core-excited parent ions relax via Auger decay [39,40], resulting in multiply charged product ions. These photoions are extracted from the ion trap by a pulsed exit aperture potential, and ion bunches are focused into the first acceleration stage of a pulsed Wiley-McLaren reflectron time-of-flight mass spectrometer, where ion-yield spectra are recorded while scanning the incident photon energy across the $L_{2,3}$ absorption edges. Doubly and triply charged product ions were detected preferentially in photoionization mass spectra, since these were the most intense species at settings which optimized trapping efficiency and transmission for parent and product ions.

As can be seen from Fig. 1, the partial ion-yield channels of doubly and triply charged product ions produce nearly identical spectra when scaled to the same intensity. Since the individual partial ion-yield spectra are very similar for a given transition-metal cation studied here, these partial ion-yield spectra can be assumed to be proportional to the total ion yield and thus to the x-ray-absorption cross section. Although the restriction to doubly and triply charged product ions might introduce an uncertainty in the relative intensities of the transitions, the excitation energies are not affected. For calcium, this procedure is even exact, because the generation of higher-charge states does not contribute significantly to the total ion yield, as can be rationalized from Auger decay of the $2p$ core hole. Doubly charged cations will be generated in *LVV* Auger decay, whereas triply charged cations stem from *LMM* and *MMV* or *MVV* Auger cascades. Partial ion-yield detection of $2p$ x-ray-absorption of calcium [41] and scandium [23] atoms also found doubly and triply charged cations to account for ≈95% of the total ion yield. A typical $2p$ photoionization mass spectrum of calcium cations is given in the inset of Fig. 1.

All spectra presented here were obtained at the Berlin synchrotron radiation facility BESSY II beamlines U49/2-PGM-1 and UE52-SGM. Photon energies were calibrated with the neon $1s$ x-ray-absorption spectrum recorded in first, second, and third order of the monochromator grating. Absolute photon energies at U49/2-PGM-1 are calibrated within 200 meV. Only the spectra of vanadium and cobalt ions in their ground-state configurations, which were recorded at UE52-SGM, have a larger absolute uncertainty of 2 eV.

B. State-selective x-ray spectroscopy

X-ray-absorption spectroscopy monitors photon-induced electronic transitions between initial and final states. Since gas discharges, as in the metal ion source used here, typically produce ions in metastable excited states by electron impact or Penning ionization [42–44], transition-metal cations are generated in different initial states, each of which would allow transitions to all final states accessible in dipole transitions with finite transition matrix elements. The data presented here were obtained selectively on $3d$ transition-metal ions in their ground states by quenching excited states prior to x-ray

TABLE I. Ground state configurations of $3d$ transition-metal atoms and cations, including calcium [52–63]. Bond dissociation energies D_0 are given for argon complexes of the cations [45–51].

	Atom	Reference	Cation	Reference	D_0	Reference
Ca	$[Ar]3d^{0}4s^{2}$	[55]	$[Ar]3d^{0}4s^{1}$	[63]		
Sc	$[Ar]3d^{1}4s^{2}$	[55]	$[Ar]3d^{1}4s^{1}$	[55]		
Ti	$[Ar]3d^{2}4s^{2}$	[58]	$[Ar]3d^{2}4s^{1}$	[55]		
V	$[Ar]3d^{3}4s^{2}$	[53]	$[Ar]3d^{4}4s^{0}$	[56]	381 meV	[46]
Cr	$[Ar]3d^{5}4s^{1}$	[55]	$[Ar]3d^{5}4s^{0}$	[55]	270 meV	[48,49]
Mn	$[Ar]3d^{5}4s^{2}$	[55]	$[Ar]3d^{5}4s^{1}$	[55]		
Fe	$[Ar]3d^{6}4s^{2}$	[60]	$[Ar]3d^{6}4s^{1}$	[54]	110 meV	[50]
Co	$[Ar]3d^{7}4s^{2}$	[61]	$[Ar]3d^{8}4s^{0}$	[62]	508 meV	[47]
Ni	$[Ar]3d^{8}4s^{2}$	[59]	$[Ar]3d^{9}4s^{0}$	[52]	550 meV	[45]
Cu	$[Ar]3d^{10}4s^{1}$	[57]	$[Ar]3d^{10}4s^{0}$	[57]	490 meV	[51]

absorption. Two different approaches, argon complex formation or relaxation of metastable states, were followed to reduce the number of initial-state configurations: For 3d transition-metal ions with large binding energy to argon [45–51] on the order of 270–550 meV listed in Table I, the formation of argon complexes in the liquid-nitrogen-cooled metal ion source is an efficient means to quench metastable excited states. This was applied to vanadium, cobalt, nickel, and copper cations, where the binding energy in the $3d^{n+1}4s^0$ configuration is larger than in the $3d^n4s^1$ configuration [51], thus selecting metal cations in their electronic ground states. In addition to ground-state preparation, these argon complexes also quench higher-charge states of the transition-metal product ion in the Auger decay following 2p x-ray absorption by charge transfer to the rare-gas atom.

Alternatively, preparation of ground-state ions can also be achieved by setting the residence time inside the radio-frequency ion trap to 1–10 s, i.e., much longer than the excited-state lifetime [31]. If the ion trap is loaded continuously and is filled already 1–2 s before x-ray photons are admitted, most of the ions will have relaxed to their ground states. This relaxation of excited electronic states was applied in the investigation of calcium, titanium, chromium, manganese, and iron cations, for which argon complexes are less efficiently formed in the metal ion source. In both approaches, thermal repopulation of excited electronic states within the same configuration is avoided by buffer-gas cooling to liquid-nitrogen temperature.

C. 2p x-ray-absorption spectra of 3d transition-metal ions

An overview of the 2p photoionization spectra of 3d transition-metal cations from scandium through copper is given in Fig. 2. Although it is not part of the 3d transition-metal series, calcium was included because of its ionic $[\mathrm{Ar}]3d^04s^1$ ground-state configuration.

Since the spatial overlap of 2p and 3d states is much larger than that of 2p and 4s states, $\langle 2p|r|3d\rangle^2 \gg \langle 2p|r|4s\rangle^2$, x-ray absorption at the 2p edges of 3d transition metals is dominated by transitions into unoccupied 3d states, and $2p \rightarrow 4s$ transitions contribute only weakly to the spectra. Therefore, a close resemblance of 2p x-ray photoionization spectra of atoms [20–26,28,29] and their corresponding cations is expected and indeed observed for 3d transition metals with identical cationic and atomic ground-state 3d configurations [64]. This is true for all transition metals except for vanadium, cobalt, and nickel, where atomic and cationic 3d occupations differ by one electron because of 4s to 3d promotion, as can be seen from the compilation of electronic ground-state configurations [52–62] in Table I.

Apart from their similar spectral shape, the 2p excitation energies are nearly identical for atoms and cations of the same element, although differences in the first and second ionization potentials are on the order of 10 eV. In the ionic ground states of 3d transition metals, listed in Table I, a 4s electron is removed from the atom and a second 4$s$electron might be transferred to 3d states. Since neither 2p core-level nor 3d valence-electron wave functions possess radial nodes, their mean radii are very similar. Therefore the 2p and 3d electron binding energy is affected in much the same way by the change of the intra-atomic Coulomb potential when a 4s electron is removed upon ionization. Hence, the excitation energy of 2p to 3d transitions is not expected to differ for 3d transition-metal atoms and cations.

Because of well-resolved multiplet structures in the 2p x-ray-absorption spectra, an analysis based on Hartree-Fock calculations [3,9,11,12] and the $Z + 1$ approximation can be performed to assign initial and final states of 3d transition-metal ions. Hartree-Fock calculations were carried out with the MISSING program package. For comparison to the experimental data, stick spectra were broadened with a natural linewidth of 200 meV and a Gaussian according to the actual experimental broadening of 50–250 meV, given below individually for each element. Calculated spectra were shifted by 1–2 eV to match the experimental excitation energies. All spectra were calculated for 100 K ion temperature, corresponding to the experimental conditions. The multiplet structure of the 2p photoionization spectra will be discussed in detail in the following.

1. Calcium

The x-ray-absorption spectrum of calcium cations in Figs. 1 and 2 was recorded with an energy resolution of 100 meV. It shows two distinct 2p spin-orbit-split features, as would be expected for the ionic ground state with $[\mathrm{Ar}]3d^04s^1$ initial-state configuration. The lines visible in Figs. 1 and 2 can thus be reproduced by Hartree-Fock calculations with transitions into $2p^53d^14s^1$, $2p^53d^04s^2$, and $2p^53d^04s^14d^1$ final states as shown in Fig. 1. Transitions into 3d states dominate the spectrum and lead to intense resonances at 348.9 and 352.2 eV, separated by the calcium 2p spin-orbit splitting of 3.3 eV, which agrees with reported values of 3.1–3.6 eV [24,65–67], while the weaker lines at 359.0 and 361.5 eV can be ascribed to transitions into 4d states, in agreement with the assignment for calcium atoms [24,41] which show a very similar 2p x-ray-absorption spectrum.

2. Scandium and titanium

Scandium and titanium show 2p x-ray-absorption spectra which are dominated by very complex multiplet structures in the final state, typical for highly correlated open-shell systems. The photon energy resolution used here is 50 meV for scandium and 125 meV for titanium. Since the width of this multiplet splitting is comparable to the 2p spin-orbit splitting of 4.5 eV in scandium [23] and 6.2 eV in titanium [68], transitions involving $2p_{3/2}$ and $2p_{1/2}$ core-hole states overlap strongly, and the spectra cannot be separated into L_3 and L_2 edge transitions. Comparison to Hartree-Fock calculations shows that scandium and titanium cations were prepared in their electronic ground states with $[\mathrm{Ar}]3d^14s^1$ and $[\mathrm{Ar}]3d^24s^1$ initial-state configurations, respectively. The 2p spectra of scandium and titanium cations agree well with those of the corresponding neutral atoms [23,29] because of their identical 3d electron configurations. Therefore, the assignment of atomic transitions [23,29] also applies to the cations.

3. Vanadium

Vanadium cations were investigated as V^+-Ar complexes with a binding energy of 380 meV [46]. With this argon

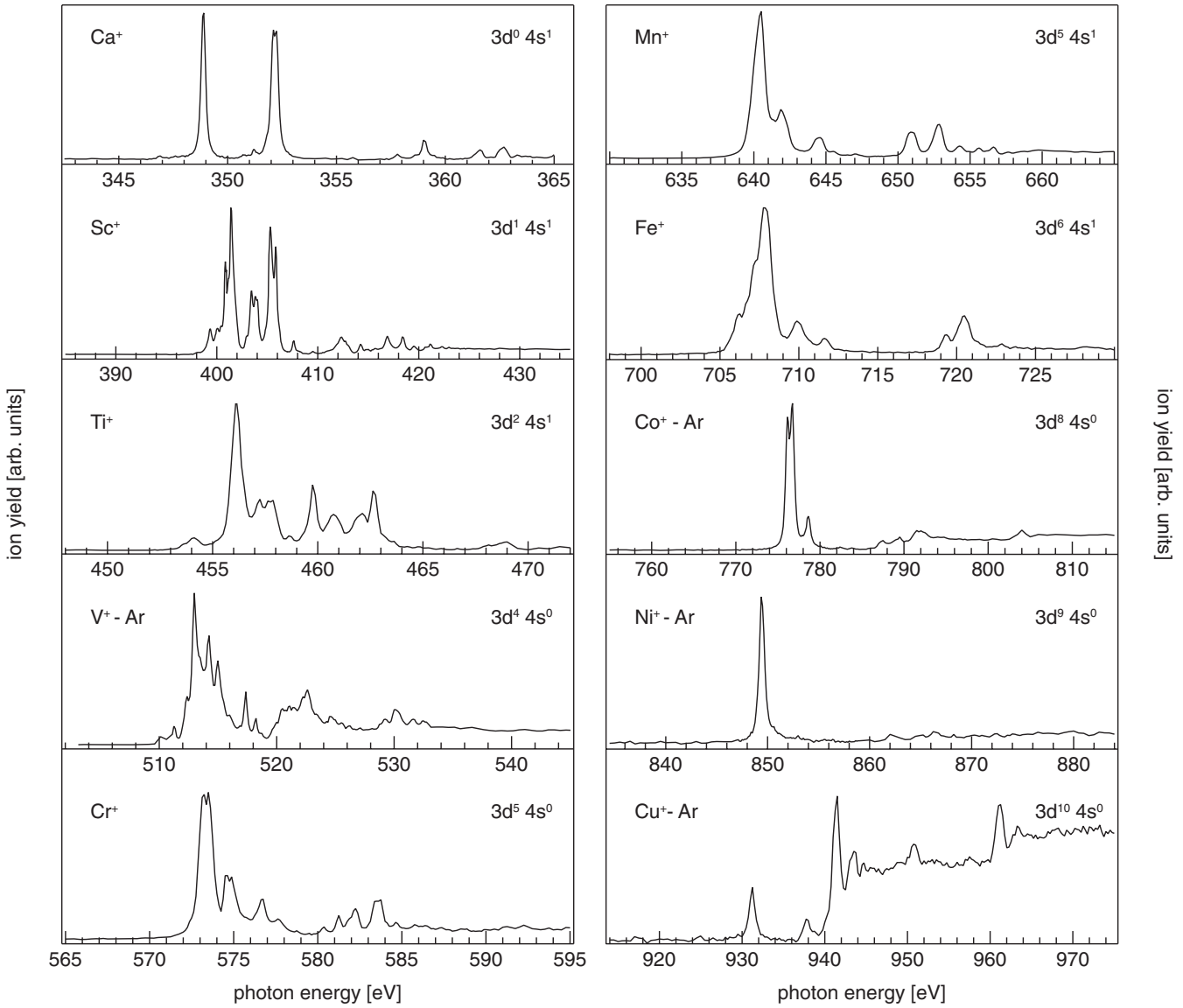

FIG. 2. Experimental x-ray-absorption spectra recorded at the $L_{2,3}$ edges of 3*d* transition-metal ions in their ground-state configurations from scandium through copper, including calcium.

complex formation, the [Ar]$3d^4 4s^0$ ground state of the vanadium cation was studied, because the [Ar]$3d^3 4s^1$ excited state has a lower binding energy to argon [51]. However, bare vanadium cations were additionally prepared in the metastable [Ar]$3d^3 4s^1$ initial-state configuration. The $2p$ spectra for vanadium cations in their ground and excited states, both recorded with a photon energy resolution of 100 meV, are compared in Fig. 3, demonstrating the efficiency of argon complex formation in ground-state preparation. Since these two spectra were taken at two different beamlines with different uncertainties in energy calibration, the absolute energies are not expected to match. The experimental spectrum of the ground-state configuration in V^+-Ar, shown in the upper panel of Fig. 3, can be reproduced by Hartree-Fock calculations with transitions into $2p^5 3d^5 4s^0$ and $2p^5 3d^4 4s^1$ final states. Since the 3*d* occupations in vanadium atoms and cations in their ground states differ by one electron, their $2p$ x-ray-absorption spectra differ as well.

Calculations accounting for transitions into $2p^5 3d^4 4s^1$ and $2p^5 3d^3 4s^2$ final states reproduce the experimental spectrum of the metastable parent ion configuration in bare vanadium cations with good agreement in the 510–525 eV range, as is evident from the lower panel in Fig. 3. Since this excited initial-state configuration corresponds in 3*d* occupancy to the vanadium atom, their x-ray-absorption spectra are nearly identical [29]. In neither configuration could a series of transitions around 527–532 eV be reproduced by Hartree-Fock calculations with the Cowan code because of the limited size of the matrix; these lines are very likely due to transitions into 4*d* and 5*d* orbitals.

4. Chromium and manganese

Chromium and manganese, with their half-filled 3*d* subshells, exhibit qualitatively similar spectra in Fig. 2 since both adopt high-spin initial states with [Ar]$3d^5 4s^0$ $^6S_{5/2}$ and [Ar]$3d^5 4s^1$ $^7S_3$ ground-state configurations, respectively.

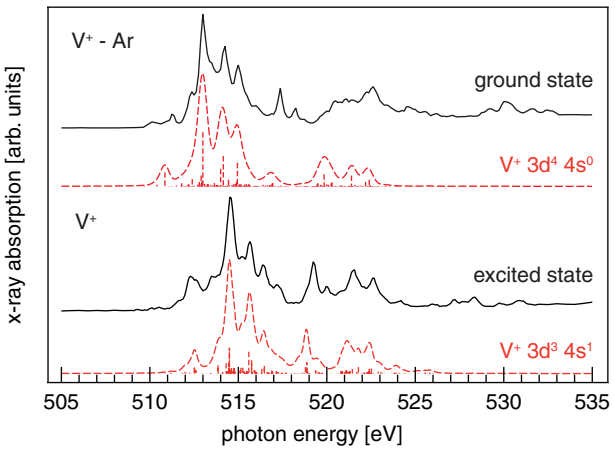

FIG. 3. (Color online) 2p photoionization spectra of V^+-Ar complexes and V^+, compared to Hartree-Fock calculations for $[Ar]3d^4 4s^0$ and $[Ar]3d^1 4s^1$ initial-state configurations. The ground state spectrum (absolute uncertainty 2 eV) has been aligned to the excited state spectrum (absolute uncertainty 200 meV) to match the relative energies of the Hartree-Fock results.

These exceptionally stable ^6S states of the localized $3d^5$ configurations persist even in the cationic chromium and manganese dimers [34], as well as in impurity atoms and thin films [69], whose 2p spectra are nearly identical to the atomic [20,22] and ionic 2p spectra. The photon energy resolution is 125 meV for the chromium and manganese spectra in Fig. 2.

Ground-state preparation for chromium cations was carried out by relaxing metastable states in the ion trap. This is illustrated in Fig. 4. The upper panel of Fig. 4 shows an x-ray-absorption spectrum of chromium cations where the residence time $t = 1$–10 s in the ion trap was tuned above the lifetime of the excited-state configuration, and an additional 2 s delay was introduced between loading the trap and irradiating the ions at every photon energy step. Consequently, Hartree-

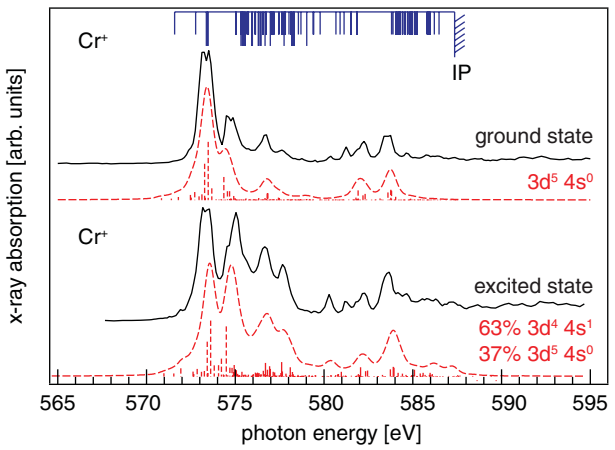

FIG. 4. (Color online) Preparation of ground-state chromium cations in the radio-frequency trap. Upper panel: pure $[Ar]3d^5 4s^0$ ground state at $t \gg 1$ s residence time. Additionally shown, $Z + 1$ approximation [55] for chromium ground state (the long sticks correspond to transitions into 3d states, the shorter ones to all other dipole-allowed transitions). Lower panel: 63% $[Ar]3d^4 4s^1$ excited state and 37% $[Ar]3d^5 4s^0$ ground state at $t \ll 1$ s residence time.

Fock calculations with transitions from a single $[Ar]3d^5 4s^0$ initial-state configuration into $2p^5 3d^6 4s^0$ and $2p^5 3d^5 4s^1$ final states reproduce the experimental chromium cation spectrum in the upper panel of Fig. 4. Hence all chromium cations were prepared in their ground-state $[Ar]3d^5 4s^0$ configuration. The weak lines around 581 eV are attributed to contributions from $2p^5 3d^5 4d^1$ and $2p^5 3d^5 5s^1$ final states in the $Z + 1$ approximation [55], also shown in Fig. 4. Because of the identical $3d^5$ initial-state configuration, the spectra and excitation energies are very similar for chromium atoms [20,22] and cations.

For the spectrum in the lower panel of Fig. 4, the ion trap was not filled continuously but the radio frequency was switched on only when photoionization mass spectra were taken at each photon energy step. In addition, the residence time $t \ll 1$ s of chromium cations in the ion trap was shorter than the lifetime of the excited-state configuration $[Ar]3d^4 4s^1$. In this case, the chromium cations could not relax before the shutter was opened to record the photoionization spectra. The resulting 2p photoionization spectrum can be reproduced by Hartree-Fock calculations for two initial-state configurations with 37% $[Ar]3d^5 4s^0$ ground-state and 63% $[Ar]3d^4 4s^1$ metastable-state contribution. Thus only 37% of the chromium cations were found to adopt the ground-state configuration in this case.

Likewise, manganese cations were prepared in their $[Ar]3d^5 4s^1$ ground-state configuration. Although the cationic and atomic [20] 2p x-ray-absorption spectra again agree very well in their line shapes, they differ in excitation energy by approximately 1 eV for manganese.

5. Iron and cobalt

The 2p photoionization spectra of iron and cobalt show fewer lines than those of the early transition metals because the number of accessible final states decreases as the 3d shell is closed along the series. These spectra were recorded with a photon energy resolution of 125 meV for iron and 250 meV for cobalt. Because of their equal 3d occupancy, the x-ray-absorption spectrum of ground-state $[Ar]3d^6 4s^1$ iron cations is nearly identical to that of iron atoms [28], and the assignment of atomic transitions [28,29] will also hold for the cation.

This is not true for cobalt cations, whose $[Ar]3d^8 4s^0$ ground state differs in 3d occupation from the atomic $[Ar]3d^7 4s^2$ ground state. Cobalt cations were prepared as Co^+-Ar complexes with a bond dissociation energy of 508 meV [47] for the $[Ar]3d^8 4s^0$ configuration. A Hartree-Fock calculation reproduces the experimental spectrum and confirms the $[Ar]3d^8 4s^0$ ground state for this Co^+-Ar complex.

6. Nickel

Nickel cations were prepared as argon complexes with a bond dissociation energy of 550 meV [45], the largest in the 3d transition-metal series. The 2p photoionization spectra of nickel-argon complexes Ni^+-Ar and Ni^+-Ar_2 in their ground-state configurations were recorded with 125 meV photon energy resolution. For both complexes, a single L_3 line emerges at 849.4 eV, as would be expected for an $[Ar]3d^9 4s^0\ ^2D_{5/2}$ initial state. In the $2p^5 3d^{10} 4s^0$ final-state configuration, $2p_{1/2}$ and $2p_{3/2}$ core holes would lead to $^2P_{1/2}$ and $^2P_{3/2}$ terms. In a dipole transition with $\Delta J = 0, \pm 1$, however, only the $2p^5 3d^{10} 4s^0\ ^2P_{3/2}$ final state can be reached

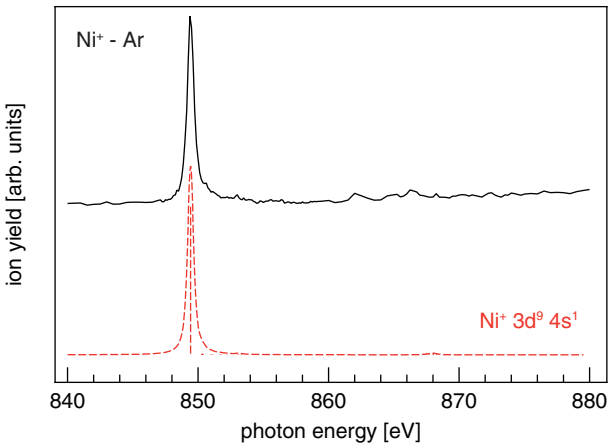

FIG. 5. (Color online) Experimental $2p$ photoionization spectrum of Ni^+-Ar complexes (solid line) compared to a calculated $2p$ x-ray-absorption spectrum (without continuum excitation) for the $[Ar]3d^9 4s^0$ initial-state configuration (dashed line).

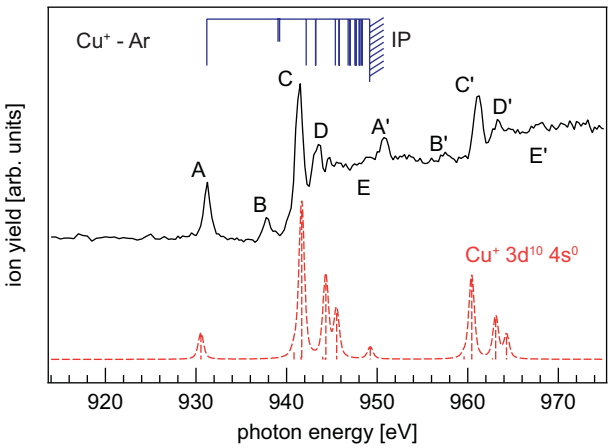

FIG. 6. (Color online) Experimental Cu^+-Ar $2p$ photoionization spectrum (solid line) compared to the calculated spectrum for the $[Ar]3d^{10}4s^0$ initial-state configuration and to results of the $Z+1$ approximation [55].

from the $^2D_{5/2}$ initial state, which leads to a suppression of the L_2 line, leaving a single L_3 line as the prominent feature in the spectrum. Additional transitions into $4s$ states with $2p^5 3d^9 4s^1$ final-state configurations lead to weak lines at the L_2 edge.

A comparison of the experimental $2p$ photoionization spectrum of the Ni^+-Ar and Ni^+-Ar_2 complexes to a Hartree-Fock calculation of nickel cations with $2p^5 3d^{10} 4s^0$ and $2p^5 3d^9 4s^1$ final-state configurations in Fig. 5 shows that for both species the initial state is the unperturbed $[Ar]3d^9 4s^0$ configuration, which is also the ground state of the nickel cation. Thus the argon atom, although bound to the nickel cation with a bond dissociation energy of 550 meV, quenches excited states to the ground state but does not otherwise affect the electronic structure of the nickel cation, which is also in agreement with laser photodissociation studies on Ni^+-Ar [45].

Since the $[Ar]3d^9 4s^0$ ground state of nickel cations is different from the $[Ar]3d^8 4s^2$ ground state of nickel atoms, their $2p$ x-ray-absorption spectra cannot be expected to agree [25]; even more so as thermal evaporation of nickel atoms in crossed-beam experiments leads to mixed $[Ar]3d^8 4s^2$ and $[Ar]3d^9 4s^1$ initial-state configurations [25].

7. Copper

In the case of ground-state copper cations with $[Ar]3d^{10}4s^0$ initial state, prepared as Cu^+-Ar complexes with 490 meV binding energy [51], the $3d$ shell is fully occupied, hence the spectrum is dominated by transitions into continuum $(\epsilon s, \epsilon d)$ and bound (ns, nd) final states with $n \geqslant 4$. Because of the small overlap of $2p$ and (ns, nd) states, continuum and resonant excitations contribute with almost equal absorption cross sections to the experimental spectrum, as can be seen in Figs. 2 and 6.

The $2p$ x-ray-absorption spectrum of ground-state copper cations, recorded with 250 meV photon energy resolution, shown in Figs. 2 and 6, exhibits two steps visible at 942.0 and 961.75 eV, corresponding to the L_3 and L_2 edges in the $2p$ photoionization spectrum. These steps exhibit an intensity ratio of nearly 2:1 as would be expected for direct $2p$ photoionization. This simple interpretation as continuum steps is, however, misleading, since the resulting $2p_{3/2}$ photoionization threshold of 942.0 eV for copper cations would be too low compared to the semiempirical threshold of 939.5 eV obtained from atomic copper $2p$ photoionization [21] and the $2p_{3/2}$ binding energy of 940.5 eV obtained for copper atoms by x-ray photoelectron spectroscopy [29]. Instead, the direct $2p$ photoionization threshold is obscured by resonant transitions into Rydberg states, as will be shown in the following for the case of copper.

D. Detailed analysis of copper $2p$ photoexcitation

Individual final states can be extracted from Hartree-Fock calculations, which is done for $2p$ photoionization of copper cations because the experimental spectrum shows a detailed structure which was not observed in $2p$ x-ray absorption of copper atoms [21]. In our calculations, the initial-state configuration was assumed to be the cationic ground state, $[Ar]3d^{10}4s^0$, which is in good agreement with the experimental spectrum. $2p^5 3d^{10} 4s^1$, $2p^5 3d^{10} 4d^1$, and $2p^5 3d^{10} 5d^1$ final-state configurations reproduce the resonant excitations in the $2p$ photoionization spectrum fairly well and allow assignment of individual lines. Continuum excitation was not accounted for in the calculated spectrum.

Peak A at 931.25 eV in Fig. 6 is a transition into a $2p^5 3d^{10} 4s^1\ ^1P_1$ final state, with peak A' a transition into a $^3P_1$ final state 19.5 eV higher in energy, its corresponding spin-orbit-split partner. In general, the $2p$ spin-orbit splitting of 19.75 eV derived from analysis of the $2p$ photoionization spectrum agrees well with the 19.64 eV obtained from x-ray photoelectron spectroscopy of copper atoms [70]. Peak B cannot be reproduced by Hartree-Fock calculations at the Cowan code level used here, either by taking further final-state configurations into account or by including excited initial states. However, lines B at 937.75 eV and B' at 957.5 eV are separated by 19.75 eV, suggesting B' to be the spin-orbit-split partner of B. This line is tentatively assigned to a small contribution (less than 3% as estimated from its intensity relative to the continuum excitation) of the $[Ar]3d^9 4s^1$ initial state, suggested by the $Z+1$ approximation [55] shown

in Fig. 6. Peak C at 941.5 eV is due to transitions into 4d-orbital-derived $^3P_1$ and $^1P_1$ final states with the spin-orbit-split partner C' a $^3D_1$ final state 19.75 eV higher in energy. Another spin-orbit-split pair separated by 19.75 eV are the lines D at 943.5 eV and D' at 963.25 eV, which originate from transitions into 5d orbitals, where D can be attributed to $^3P_1$ and $^1P_1$ final states, while D' is a $^3D_1$ final state. The faint transitions E at 947.5 eV and E' at 967 eV are presumably spin-orbit-split partners with a separation of 19.5 eV, but cannot be reproduced in the Hartree-Fock calculation. However, coinciding in energy with the ionization potential derived from the $Z+1$ approximation in Fig. 6, E and E' are presumably the onsets of direct photoionization at the spin-orbit-split 2p levels. This implies that the absorption intensity below peak E arises from resonant excitation into very dense Rydberg (ns,nd) states masking the photoionization threshold. Therefore, the prominent step edges visible at 942.0 and 961.75 eV are not caused by the direct photoionization threshold, which is 5.5 eV higher in excitation energy, but by resonant transitions into bound states. This has implications for the analysis of 2p x-ray magnetic circular dichroism (XMCD) spectra [71,72] of 3d transition elements, where two step functions [73] are subtracted from the isotropic 2p x-ray-absorption spectrum to remove the L_3 and L_2 edge jumps for normalization of the XMCD asymmetry: These step functions should not be set to the direct 2p photoionization threshold since transitions into ns and nd ($n \geqslant 4$) states should also be removed from the spectrum to account only for the intensity of $2p \rightarrow 3d$ transitions. While these might be very close in energy for bulk metals and even free atoms, they may differ by 10 eV in free atomic or cluster ions, as we have shown here for the case of copper. In light of these results, the empirical approach in x-ray magnetic circular dichroism spectroscopy of placing the edge thresholds to the peak positions of the L_3 and L_2 lines [73] is justified for bulk metals as well as for ions and atoms.

E. $2p_{3/2}$ core-hole lifetime in nickel cations

Since there is only one single L_3 line at 849.4 eV in the 2p x-ray-absorption spectrum spectrum of nickel cations, attributed to a transition from their [Ar]$3d^9 4s^0\ ^2D_{5/2}$ ground state to a $2p^5 3d^{10} 4s^0\ ^2P_{3/2}$ final state, the lifetime of this $2p_{3/2}$ core excited state can be extracted from the experimental data by fitting a Voigt profile with a 125 meV Gaussian and a Lorentzian with full width at half maximum of 0.40 ± 0.01 eV to the L_3 line. The resulting lifetime of 1.6 ± 0.1 fs is slightly larger than the value of 1.4 fs observed in bulk nickel [74] and 1.3 fs which can be estimated from the L_3 line full width at half maximum of 0.52 eV for nickel impurities on potassium films [5]. The reduced linewidth in nickel cations can most likely be ascribed to the absence of inhomogeneous broadening, which might be present in the case of Ni/K films because of different adatom sites.

F. Oscillator strength and unoccupied 3d states

In the dipole approximation and the Kramers-Heisenberg relation, the oscillator strength in x-ray absorption is given by the product of the square of the dipole matrix element $|\langle\phi_f|T|\phi_i\rangle|^2$ between the initial ϕ_i and final ϕ_f states, and the density of final states $\rho(E)$,

$$I \propto \frac{2\pi}{\hbar}|\langle\phi_f|T|\phi_i\rangle|^2\rho(E).$$

Successive population of 3d orbitals along the 3d series leads to a decrease of the number of empty 3d states $\rho(E)$ and therefore to a reduction of the $2p \rightarrow 3d$ oscillator strength I.

The oscillator strength can be obtained by integrating over all $2p \rightarrow 3d$ transitions at the $L_{2,3}$ edges [64,75–77]. For this analysis, the photoionization spectra were normalized to the direct ionization continuum to correct for varying target density in the ion trap, and two continuum step functions were subtracted to separate resonant from direct photoionization and to account for transitions into higher (ns,nd) states, in accordance with the results given above. The resulting oscillator strength is shown in Fig. 7 as a function of the number of unoccupied 3d states for the initial-state configurations observed experimentally. The nearly linear dependence observed in Fig. 7 is in qualitative agreement with corresponding bulk data [75–77], and underlines that the transition matrix elements for all 3d transition-metal cations should be very similar, and the oscillator strength mainly depends on the unoccupied density of states.

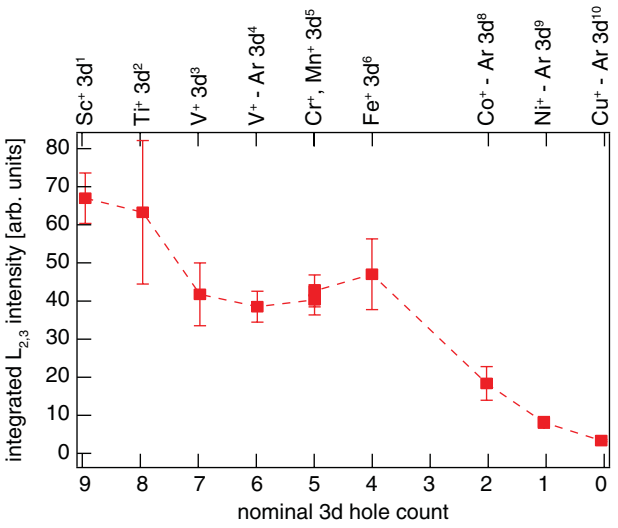

FIG. 7. (Color online) Oscillator strength of $2p \rightarrow 3d$ transitions versus nominal d-hole count (bottom axis) and element (top axis).

IV. CONCLUSION

Photoionization spectroscopy in a linear radio-frequency ion trap can be used to selectively obtain core-level excitation spectra of ions either relaxed to their electronic ground state or prepared in metastable excited states. With this technique, the photon energy range of free-metal-ion core-level excitation is expanded to deeper core levels that were not previously accessed. This allowed us to record 2p photoionization spectra of transition-metal ions across the complete 3d series. Free 3d transition-metal atoms and ions with the same 3d occupancy show nearly identical 2p x-ray-absorption spectra with nearly identical 2p excitation energies. The case of closed-3d-shell

copper cations reveals that the continuum step edge in $2p$ x-ray absorption of $3d$ transition metals does not coincide with the direct $2p$ photoionization threshold but is due to transitions into dense Rydberg states. The $2p$ photoionization spectra of $3d$ transition-metal cations presented here might serve as experimental reference spectra for dilute $3d$ transition-metal impurities or for $3d$ ions in compounds, whose electronic structure is often determined experimentally by the analysis of multiplet split $2p$ x-ray-absorption spectra. The technique of argon complex formation might also be used for ground-state preparation and alignment of their magnetic moments in x-ray magnetic circular dichroism spectroscopy of isolated atomic ions.

ACKNOWLEDGMENTS

Beam time for this project was provided by BESSY II at beamlines U49/2-PGM-1 and UE52-SGM. BESSY II is operated by Helmholtz-Zentrum Berlin. Technical assistance and user support by O. Schwarzkopf, R. Follath, H. Pfau, and G. Reichardt are gratefully acknowledged. We are grateful to P. Zimmermann for fruitful discussions.

[1] J. J. Rehr and R. C. Albers, Rev. Mod. Phys. **72**, 621 (2000).
[2] P. Glatzel and U. Bergmann, Coord. Chem. Rev. **249**, 65 (2005).
[3] F. de Groot, Coord. Chem. Rev. **249**, 31 (2005).
[4] J. Fink, T. Müller-Heinzerling, B. Scheerer, W. Speier, F. U. Hillebrecht, J. C. Fuggle, J. Zaanen, and G. A. Sawatzky, Phys. Rev. B **32**, 4899 (1985).
[5] P. Gambardella, S. S. Dhesi, S. Gardonio, C. Grazioli, P. Ohresser, and C. Carbone, Phys. Rev. Lett. **88**, 047202 (2002).
[6] T. Haupricht, R. Sutarto, M. W. Haverkort, H. Ott, A. Tanaka, H. H. Hsieh, H.-J. Lin, C. T. Chen, Z. Hu, and L. H. Tjeng, Phys. Rev. B **82**, 035120 (2010).
[7] M. Abbate, J. C. Fuggle, A. Fujimori, L. H. Tjeng, C. T. Chen, R. Potze, G. A. Sawatzky, H. Eisaki, and S. Uchida, Phys. Rev. B **47**, 16124 (1993).
[8] J. Schlappa, C. Schüßler-Langeheine, C. F. Chang, H. Ott, A. Tanaka, Z. Hu, M. W. Haverkort, E. Schierle, E. Weschke, G. Kaindl, and L. H. Tjeng, Phys. Rev. Lett. **100**, 026406 (2008).
[9] R. D. Cowan, *The Theory of Atomic Structure and Spectra* (University of California Press, Berkeley, 1981).
[10] G. van der Laan and I. W. Kirkman, J. Phys.: Condens. Matter **4**, 4189 (1992).
[11] G. van der Laan and B. Thole, J. Electron Spectrosc. Relat. Phenom. **86**, 57 (1997).
[12] A. Kotani, J. Electron Spectrosc. Relat. Phenom. **100**, 75 (1999).
[13] N. Berrah, J. D. Bozek, A. A. Wills, G. Turri, H.-L. Zhou, S. T. Manson, G. Akerman, B. Rude, N. D. Gibson, C. W. Walter, L. VoKy, A. Hibbert, and S. M. Ferguson, Phys. Rev. Lett. **87**, 253002 (2001).
[14] H. Kjeldsen, F. Folkmann, T. S. Jacobsen, and J. B. West, Phys. Rev. A **69**, 050501 (2004).
[15] J. E. Hansen, H. Kjeldsen, F. Folkmann, M. Martins, and J. B. West, J. Phys. B **40**, 293 (2007).
[16] N. Berrah, R. C. Bilodeau, J. D. Bozek, I. Dumitriu, D. Toffoli, and R. R. Lucchese, Phys. Rev. A **76**, 042709 (2007).
[17] R. C. Bilodeau, I. Dumitriu, N. D. Gibson, C. W. Walter, and N. Berrah, Phys. Rev. A **80**, 031403 (2009).
[18] A. L. D. Kilcoyne, A. Aguilar, A. Müller, S. Schippers, C. Cisneros, G. Alna'Washi, N. B. Aryal, K. K. Baral, D. A. Esteves, C. M. Thomas, and R. A. Phaneuf, Phys. Rev. Lett. **105**, 213001 (2010).
[19] I. Dumitriu, R. C. Bilodeau, T. W. Gorczyca, C. W. Walter, N. D. Gibson, A. Aguilar, Z. D. Pešić, D. Rolles, and N. Berrah, Phys. Rev. A **81**, 053404 (2010).
[20] U. Arp, F. Federmann, E. Källne, B. Sonntag, and S. L. Sorensen, J. Phys. B **25**, 3747 (1992).
[21] U. Arp, K. Iemura, G. Kutluk, M. Meyer, T. Nagata, M. Sacchi, B. Sonntag, S. Yagi, and A. Yagishita, J. Phys. B **27**, 3389 (1994).
[22] U. Arp, K. Iemura, G. Kutluk, T. Nagata, S. Yagi, and A. Yagishita, J. Phys. B **28**, 225 (1995).
[23] B. Obst, T. Richter, M. Martins, and P. Zimmermann, J. Phys. B **34**, L657 (2001).
[24] B. Obst, J. E. Hansen, B. Sonntag, P. Wernet, and P. Zimmermann, Phys. Rev. A **65**, 062716 (2002).
[25] K. Godehusen, T. Richter, P. Zimmermann, and M. Martins, Phys. Rev. Lett. **88**, 217601 (2002).
[26] M. Martins, K. Godehusen, T. Richter, and P. Zimmermann, in *X-Ray and Inner-Shell Processes,* edited by A. Bianconi, A. Marcelli, and N. L. Saini, AIP Conf. Proc. No. **652** (AIP, New York, 2003), p. 153.
[27] G. Prümper, S. Kröger, R. Müller, M. Martins, J. Viefhaus, P. Zimmermann, and U. Becker, Phys. Rev. A **68**, 032710 (2003).
[28] T. Richter, K. Godehusen, M. Martins, T. Wolff, and P. Zimmermann, Phys. Rev. Lett. **93**, 023002 (2004).
[29] M. Martins, K. Godehusen, T. Richter, P. Wernet, and P. Zimmermann, J. Phys. B **39**, R79 (2006).
[30] S. D. Kravis, D. A. Church, B. M. Johnson, M. Meron, K. W. Jones, J. Levin, I. A. Sellin, Y. Azuma, N. B. Mansour, H. G. Berry, and M. Druetta, Phys. Rev. Lett. **66**, 2956 (1991).
[31] R. Thissen, J. M. Bizau, C. Blancard, M. Coreno, C. Dehon, P. Franceschi, A. Giuliani, J. Lemaire, and C. Nicolas, Phys. Rev. Lett. **100**, 223001 (2008).
[32] M. C. Simon, J. R. Crespo López-Urrutia, C. Beilmann, M. Schwarz, Z. Harman, S. W. Epp, B. L. Schmitt, T. M. Baumann, E. Behar, S. Bernitt, R. Follath, R. Ginzel, C. H. Keitel, R. Klawitter, K. Kubiček, V. Mäckel, P. H. Mokler, G. Reichardt, O. Schwarzkopf, and J. Ullrich, Phys. Rev. Lett. **105**, 183001 (2010).
[33] K. Hirsch, J. T. Lau, P. Klar, A. Langenberg, J. Probst, J. Rittmann, M. Vogel, V. Zamudio-Bayer, T. Möller, and B. von Issendorff, J. Phys. B **42**, 154029 (2009).
[34] J. T. Lau, K. Hirsch, A. Langenberg, J. Probst, R. Richter, J. Rittmann, M. Vogel, V. Zamudio-Bayer, T. Möller, and B. von Issendorff, Phys. Rev. B **79**, 241102 (2009).
[35] J. T. Lau, J. Rittmann, V. Zamudio-Bayer, M. Vogel, K. Hirsch, P. Klar, F. Lofink, T. Möller, and B. v. Issendorff, Phys. Rev. Lett. **101**, 153401 (2008).

[36] J. T. Lau, K. Hirsch, P. Klar, A. Langenberg, F. Lofink, R. Richter, J. Rittmann, M. Vogel, V. Zamudio-Bayer, T. Möller, and B. v. Issendorff, Phys. Rev. A **79**, 053201 (2009).
[37] J. T. Lau, M. Vogel, A. Langenberg, K. Hirsch, J. Rittmann, V. Zamudio-Bayer, T. Möller, and B. von Issendorff, J. Chem. Phys. **134**, 041102 (2011).
[38] M. Niemeyer, K. Hirsch, V. Zamudio-Bayer, A. Langenberg, M. Vogel, M. Kossick, C. Ebrecht, K. Egashira, A. Terasaki, T. Möller, B. v. Issendorff, and J. T. Lau, Phys. Rev. Lett. **108**, 057201 (2012).
[39] M. O. Krause, J. Phys. Chem. Ref. Data **8**, 307 (1979).
[40] M. H. Chen, B. Crasemann, and H. Mark, Phys. Rev. A **24**, 177 (1981).
[41] T. Matsuo, T. Hayaishi, Y. Itoh, T. Koizumi, T. Nagata, Y. Sato, E. Shigemasa, A. Yagishita, M. Yoshino, and Y. Itikawa, J. Phys. B **25**, 121 (1992).
[42] P. R. Kemper and M. T. Bowers, J. Phys. Chem. **95**, 5134 (1991).
[43] W. S. Taylor, E. M. Spicer, and D. F. Barnas, J. Phys. Chem. A **103**, 643 (1999).
[44] Y. Ibrahim, E. Alsharaeh, R. Mabrouki, P. Momoh, E. Xie, and M. S. El-Shall, J. Phys. Chem. A **112**, 1112 (2008).
[45] D. Lessen and P. J. Brucat, Chem. Phys. Lett. **152**, 473 (1988).
[46] D. Lessen and P. J. Brucat, J. Chem. Phys. **91**, 4522 (1989).
[47] D. Lessen and P. J. Brucat, J. Chem. Phys. **90**, 6296 (1989).
[48] D. E. Lessen, R. L. Asher, and P. J. Brucat, Chem. Phys. Lett. **177**, 380 (1991).
[49] P. R. Kemper, M. T. Hsu, and M. T. Bowers, J. Chem. Phys. **95**, 10600 (1991).
[50] B. L. Tjelta, D. Walter, and P. B. Armentrout, Int. J. Mass Spectrom. **204**, 7 (2001).
[51] G. E. Froudakis, M. Muhlhauser, S. C. Farantos, A. Sfounis, and M. Velegrakis, Chem. Phys. **280**, 43 (2002).
[52] A. G. Shenston, J. Res. Natl. Inst. Stand. Technol. A **74**, 801 (1970).
[53] D. S. Davis and K. L. Andrew, J. Opt. Soc. Am. **68**, 235 (1978).
[54] S. Johansson, Phys. Scr. **18**, 217 (1978).
[55] J. Sugar and C. Corliss, J. Phys. Chem. Ref. Data **14**, Supplement No. 2 (1985).
[56] L. Iglesias, M. I. Cabeza, and B. de Luis, Publ. Inst. Opt. Madrid **47**, 1 (1988).
[57] J. Sugar and A. Musgrove, J. Phys. Chem. Ref. Data **19**, 527 (1990).
[58] P. Forsberg, Phys. Scr. **44**, 446 (1991).
[59] U. Litzen, J. W. Brault, and A. P. Thorne, Phys. Scr. **47**, 628 (1993).
[60] G. Nave, S. Johansson, R. C. M. Learner, A. P. Thorne, and J. W. Brault, Astrophys. J. Suppl. Ser. **94**, 221 (1994).
[61] J. Pickering and A. Thorne, Astrophys. J. Suppl. Ser. **107**, 761 (1996).
[62] J. Pickering, A. Raassen, P. Uylings, and S. Johansson, Astrophys. J. Suppl. Ser. **117**, 261 (1998).
[63] D. C. Morton, Astrophys. J. Suppl. Ser. **149**, 205 (2003).
[64] G. van der Laan and B. T. Thole, Phys. Rev. B **43**, 13401 (1991).
[65] M. Meyer, E. v. Raven, M. Richter, B. Sonntag, R. D. Cowan, and J. E. Hansen, Phys. Rev. A **39**, 4319 (1989).
[66] M. Meyer, E. von Raven, B. Sonntag, and J. E. Hansen, Phys. Rev. A **49**, 3685 (1994).
[67] P. Wernet, P. Glatzel, A. Verweyen, B. Sonntag, B. Obst, W. Benten, C. Gerth, P. Zimmerman, A. Gray, and J. Costello, J. Phys. B **31**, L289 (1998).
[68] J. C. Fuggle and N. Mårtensson, J. Electron Spectrosc. Relat. Phenom. **21**, 275 (1980).
[69] P. Gambardella, L. Claude, S. Rusponi, K. J. Franke, H. Brune, J. Raabe, F. Nolting, P. Bencok, A. T. Hanbicki, B. T. Jonker, C. Grazioli, M. Veronese, and C. Carbone, Phys. Rev. B **75**, 125211 (2007).
[70] M. Martins, K. Godehusen, T. Richter, T. Wolff, and P. Zimmermann, J. Electron Spectrosc. Relat. Phenom. **137–140**, 345 (2004).
[71] B. T. Thole, P. Carra, F. Sette, and G. van der Laan, Phys. Rev. Lett. **68**, 1943 (1992).
[72] P. Carra, B. T. Thole, M. Altarelli, and X. Wang, Phys. Rev. Lett. **70**, 694 (1993).
[73] C. T. Chen, Y. U. Idzerda, H.-J. Lin, N. V. Smith, G. Meigs, E. Chaban, G. H. Ho, E. Pellegrin, and F. Sette, Phys. Rev. Lett. **75**, 152 (1995).
[74] M. O. Krause and J. H. Oliver, J. Phys. Chem. Ref. Data **8**, 329 (1979).
[75] A. L. Ankudinov, A. I. Nesvizhskii, and J. J. Rehr, J. Synchrotron Radiat. **8**, 92 (2001).
[76] D. H. Pearson, C. C. Ahn, and B. Fultz, Phys. Rev. B **47**, 8471 (1993).
[77] J. Graetz, C. C. Ahn, H. Ouyang, P. Rez, and B. Fultz, Phys. Rev. B **69**, 235103 (2004).